The Ten-Year-Old Child Neck Failure in Tension Using A Finite Element Model

Liqiang Dong, Haojie Mao, Guangyao Li, King H. Yang

Abstract Although a considerable number of adult finite element (FE) cervical spine models were developed to understand the injury mechanisms of the neck in auto crash scenarios, relatively less effort has been devoted to develop child models. Few FE cervical spine models were conducted in tensile responses, which were observed due to airbag and seatbelt interactions. In this study, a ten-year-old cervical spine FE model was developed with an aim to improve the safety of child in car crashes in future. The model geometry was obtained from medical scans and meshed using a multi-block approach. Nonlinear materials and viscoelastic materials were assigned based on literatures. The material properties were obtained mostly by scaling reported adult experimental data. The growth plate and endplate cartilage were modeled as solid elements, and element failure method was used to simulate the disc failure through pre-assigned critical stresses. Child tensile force-deformation data in three segments, Occipital-C2 (C0-C2), C4-C5 and C6-C7, were used to validate the neck model and predict failure properties. Design of computer experiments was performed to determine failure properties for intervertebral discs and ligaments. The model-predicted ultimate displacements and forces were within the experimental ranges. This study provided methods to develop a child FE neck model and to predict soft tissue failures in tension.

Keywords Finite element method, growth plate, pediatric cervical spine, tension failure

I. INTRODUCTION

Spinal injuries in children have higher morbidity and mortality compared with adults [1]. About 75% of pediatric spinal injuries are in the cervical region compared to 14% in thoracic and 11% in lumbar regions [2]. Motor vehicle crashes account for the majority of spinal injuries in the pediatric population [2]. Cervical spine injuries in children are different from those in adults, due to differences in anatomical and physiological features [3]. These differences include the relatively large head mass, ligamentous laxity, shallow angulations of facet joints, developing ossification of vertebrae and immature neck musculature [4]. Additionally, the pediatric spine has unique anatomical features like growth plate and apophyseal ring [5].

Cadaveric functional spinal unit tests [6] and cervical spinal osteoligamentous tests [7] have been performed to identify tensile properties of human pediatric subjects. However, these tests only quantify biomechanical responses; internal responses such as strain and stress cannot be calculated directly due to irregular shaped vertebrae. These internal responses are important to find out injury locations and mechanisms [8]. Finite element (FE) models can calculate these results as a numerical technique.

Many adult cervical spine FE models have been developed [9-12]. There are few pediatric cervical spine FE models reported, partially due to the lack of test data for model validation. The first pediatric human cervical spine FE model was developed by Kumaresan et al. [13]. Three C4-C6 segment models (representing one, three and six years old) were developed by scaling down an adult model of 33 years of age [14], and then adjusted for pediatric facet angles and the size of the nucleus. Effects of ossification and geometric changes were calculated by comparing flexibilities predicted by the adult and pediatric models. All respective anatomical structures, except the ligaments and annulus fibrosus (AF), used the same material properties which ranged from 57% to 89% of adult values, while different material properties for ages were not considered. The maximum forces of ligaments and the Young's modulus of annulus fibers were assumed to be 80%, 85.1% and 89.9% of the adult values while the ratio of annulus fibers to annulus ground substance was assumed 10%, 15% and 20% for the

L. Dong is a Ph.D. student specializing in Biomechanics at Hunan University in China and also affiliated with Wayne State University. H. Mao, Bioengineering Center, Wayne State University. G. Li, The State Key Laboratory of Advanced Design and Manufacturing for Vehicle

one-, three- and six-year-old models, respectively. The maximum deflections were assumed to be the same as that of an adult.

Mizuno et al. [15] developed a three-year-old total human FE model scaled from an adult model (THUMS AM50, Toyota, Japan). The basic anthropometry data were based on the dimensions of a Hybrid III dummy. The elastic modulus scaling factor of the bone was based on Irwin et al. [16]. The failure stress and strain scaling factors of bone were based on data reported by Currey et al. [17]. Material properties used to simulate soft tissues were the same as those adopted by THUMS AM50. The model was validated based on three-year-old dummy tests for the spine flexion and the chest compression, while validations of other body regions were not reported.

Scaling methodology was used in the above-mentioned child FE models. However, the detailed geometry of a child should be used for a more biofidelic model. Meyer et al. [18] developed a three-year-old child neck model based on detailed human child geometry. However, the vertebral bodies were assumed rigid and intervertebral discs were modeled as elastic materials without distinguishing the annulus and nucleus. The scaling factors selected for the mass and moment of inertia of vertebrae and the head were based on Irwin et al. [16]. Scaled experimental data of adult volunteers were used to validate the model [19]. The aforementioned child FE neck models were not validated using child experimental data. Also, none of the aforementioned child models simulated tensile responses, which were observed during airbag and seatbelt interactions.

The weight and stature of a ten-year-old child are larger than a six-year-old child (the age group for which government regulations demand deactivation of front passenger airbags) and smaller than a small adult female. For this reason, exposure to an inflating airbag for ten-year-old children is possible. Since an airbag generates tensile loading to the neck, a ten-year-old child model validated against tensile biomechanical data would be useful in the design and evaluation of age-appropriate parameters for airbag deployment. Additionally, some studies [20-22] indicate that child pedestrians 5 to 12 years of age are at the highest risk of being injured by a vehicle. For child pedestrians 8 to 12 years of age, the rate of injury per kilometer or time spent on the road, or per road crossing, was the highest compared to 3 to 7 years old (YO) and 13 to 17 YO groups [21]. These injury statistics point towards the need to have a ten-year-old biofidelic child model to study a variety of crash scenarios to derive countermeasures. In order to overcome the deficiencies in existing child cervical spine models and to improve the safety of ten-year-old children in car crashes, the aims of this study were to develop a ten-year-old FE cervical spine model based on detailed geometry of the pediatric subject and investigate the failure of soft tissues in tension.

II. METHODS

Clinical Computed Tomography (CT) and Magnetic Resonance Imaging (MRI) scans of children (10 +/- 0.5 years) treated at Children's Hospital of Michigan (CHM) were used to generate geometry of bones and skin, with approval from the Institutional Human Investigation Committee of Wayne State University. Because high quality, whole body medical scans are rarely acquired for medical diagnostic purposes, images taken from several children were used to generate the whole body geometry. Appropriate patients were identified by searching the medical records at CHM which must satisfy four conditions as described in a previous study [23]. A subject scanned with CT was selected by comparing the neck length and circumference with ten-year-old average anthropometry [24,25] to model the bones of the cervical spine. Geometries of soft tissues were based on images of adult anatomy [26,27] and child spinal models [13,18,28]. A multi-block approach, used previously for creating hexahedral meshes for body components [29-32], was adopted in this study to generate vertebral body meshes efficiently (ANSYS ICEM CFD/HEXA 12.0, Ansys, Canonsburg, PA, USA). Hypermesh 10.0 (Altair, Troy, MI) was used for the generation of remaining meshes.

Material modeling

Material laws and properties assumed for the ten-year-old child neck model are summarized in Table 1. The cancellous bone and cortical bone were modeled as isotropic elastic-plastic material (*MAT_POWER_LAW_PLASTICITY in LS-DYNA). Based on quantitative CT densities reported for the child and adult vertebral cancellous bone [33], the scaling factor for material parameters of cortical bone and cancellous

Body, Hunan University, China. K.H. Yang is Prof of Biomedical Engineering in the Bioengineering Center at Wayne State University, USA (Corresponding author, tel.: +1-313-577-0252, fax: +1-313-577-8333, E-mail address: aa0007@wayne.edu).

bone was calculated to be 0.805. Material properties of the endplates were defined as one third of those for adult cortical bones as assumed by Panzer [34] (Table 1). The growth plate was modeled as cartilaginous tissue between the vertebral body and endplate cartilage [28] (Figure 1A). The endplate cartilage was modeled using hexahedral elements.

The cancellous bone was modeled using hexahedral elements. Cortical bone and endplates were modeled using shell elements. The thicknesses of cortical bone and endplates for the adult range from 0.41 to 0.70 mm with an average of 0.5 and 0.6 mm for cortical bone and endplate, respectively [35]. Because these structures were too thin to be detected accurately from medical images, a uniform thickness of 0.37 and 0.45 mm, scaled from the adult, was assumed for the cortical bone and endplates, respectively. The scale factor was based on the dimensional scale factor GS (Table 1) reported by Mertz et al. [36].

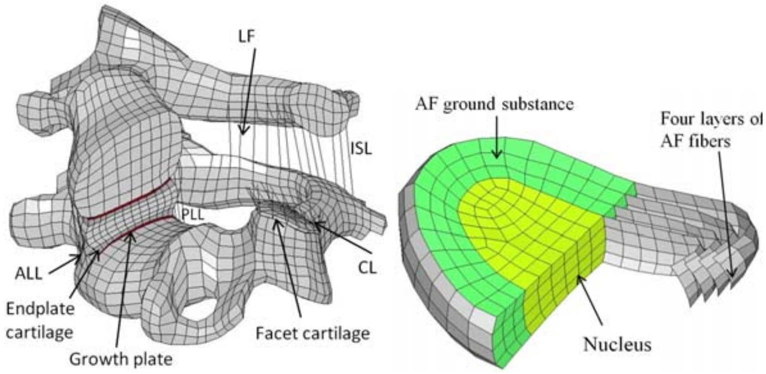

(A) (B)

Figure 1: (A) Sectioned isometric view of the C4-C5 segment model (ALL anterior longitudinal ligament; PLL posterior longitudinal ligament; CL capsular ligament; LF ligamentum flavum; ISL interspinous ligament) and (B) the three components used to represent the intervertebral disc

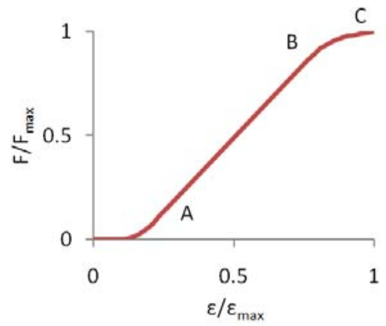

Figure 2: A typical force-deflection curve used to define the material property of ligaments. The curve was normalized by failure tensile force and deflection. C is the tolerance point, A and B define a linear region in the force-deflection curve.

TABLE 1 Material properties assumed for the ten-year-old finite element neck model and the scaling factors used to determine properties of the child

Name	Element type	Material model	Material parameters	Scaling factors [ref]	Material references
Cortical bone	Hexahedral	Isotropic elastic-plastic	E=13.44 GPa, γ=0.3 k=355 MPa, n=0.277	0.805	[37]
Cancellous bone	Quadrilateral	Isotropic elastic-plastic	E=241 MPa, γ=0.3 k=5.73 MPa, n=0.274	0.805	[38]
Endplate	Quadrilateral	Isotropic elastic-plastic	E=4.48 GPa, γ=0.3 k=118 MPa, n=0.277		
Growth plate	Hexahedral	Isotropic elastic	E=25 MPa, γ=0.4		[39-41]
Endplate cartilage	Hexahedral	Isotropic elastic	E=23.8 MPa, γ=0.4	*	[42]
Annulus ground substance	Hexahedral	Hill foam	n=2 C1=0.090 MPa, b1=4 C2=1.643 MPa, b2=-1 C3=-0.699 MPa, b3=-2	0.782[19]	[43-45]
Annulus fibers	Quadrilateral	Orthotropic elastic	Stress-stretch curve	0.782[19]	[46]
Nucleus	Hexahedral	Fluid	K=1.72 GPa	*	[47]
Facet cartilage	Hexahedral	Isotropic elastic	E=10 MPa, γ=0.4	*	[42]
Ligaments	Bar	Non-linear		0.893[19]	[48-50]
Dimensional scaling factor G_S				0.723[36]	

E, Young's modulus; γ, Poisson's ratio; k, strength coefficient; N, hardening exponent; n, C_i, b_i, material constant; K, Bulk Modulus;
* indicates the material parameters were the same as the values of adult.

The intervertebral disc is modeled into three parts as shown in Figure 1B. The ground substance of the AF was divided into three layers in the radial direction and the AF fiber laminae were represented by four layers of membrane elements. The volume of the fiber laminae was approximately 20% of the total annulus volume [51]. The cross-sectional area of the nucleus was about 50% of the total cross-sectional area of the disc [52].

The gradual change for AF fiber angle with radial position was considered in the model, with angles 25 and 155 degrees in outer layers to 45 and 135 degrees in inner layers [44,53]. The fiber reinforced model was shown in Figure 1B. The only available mechanical test data for single lamellar were from the lumber region of adult specimens reported by Holzapfel et al. [46]. The current study used the same method adopted by Panzer and Cronin [12] to interpolate the stress-stretch curves for the four simplified layers. The scaling factor reported by Yoganandan et al. [19] (Table 1) was then used to scale these curves to represent the ten-year-old lamellar properties.

The Hill foam material model available in LS-DYNA was used to model the AF ground substance. Parameters (Table 1) needed for the material model were determined based on experimental data obtained in the uniaxial tension [43], unconfined compression [44] and confined compression [45] tests on samples aligned in the radial direction. The nucleus pulposus was modeled using fluid elements with a bulk modulus of 1.72 GPa [47].

Few studies have been conducted to simulate the intervertebral discs failure in an FE model. One method was reported by DeWit and Cronin [54] for an adult C4-C5 segment. The authors used a tie-break contact between the endplate cartilage and AF with a pre-defined critical stress to mimic failure. The reason was that the majority of failure in tensile testing of bone-disc-bone specimens occurred at the endplate cartilage-AF boundary [55]. DeWit and Cronin calculated the failure tensile force for the intervertebral disc based on the average failure tensile stress reported by Kasra et al. [55]. The critical stress was then calculated by applying this failure tensile force to cross-sectional layers of AF fibers. In the current study, element failure of the growth plate and endplate cartilage was introduced through a critical stress. DeWit and Cronin's method was used to estimate the failure stresses as shown in Table 2. The failure stress of the growth plate and endplate cartilage was set at the same value. In order to calculate the failure stresses for the child, the following formulation was used to obtain the failure tensile forces for children based on adult data:

$$f' = F'_{max} * \alpha' * \alpha'_A \tag{1}$$

where F'_{max} is the failure tensile force of the intervertebral disc for adult, α' is the scaling factor for material property which was 0.782, α'_A is the cross-sectional scaling factor that is defined as the square of the dimensional scaling factor G_S which was 0.723 (Table 1). The failure forces reported by Yoganandan et al. [56] and Kasra et al. [55] were used to determine the corresponding failure stress (Table 2). As can be seen in Table 2, the failure stress calculated from the Kasra et al. study was more than twice that calculated from the Yoganandan et al. study. In order to determine a proper failure stress value, a reverse engineering approach was conducted by comparing simulation results to experimental data. More descriptions of this approach are provided in the Model validation section.

TABLE 2 Failure stress calculating based on tensile failure forces for intervertebral discs

	Failure tensile force for adult (N)	Scaled failure tensile force for child (N)	AF cross-sectional area of child (mm^2)	Failure stress for child (MPa)	Reference for failure tensile force
C4-C5	571	249.86	14.66	17.05	Yoganandan [56]
	1280	560.10		38.21	Kasra [55]
C6-C7	505	220.98	17.74	12.45	Yoganandan [56]
	1280	560.10		31.57	Kasra [55]

The ligaments were modeled using tension-only bar elements. The load-deformation curves of the ligaments had a sigmoidal shape characterized by three points as shown in Figure 2 [48,57]. The strain and force of the controlling points for each ligament were normalized by the failure strain and force respectively (Table 3). It is assumed that only the failure deflection and force were lower for the child and the shape of the force-deflection curve was retained. The failure strain and force reported for adult C2-T1 segments by Yoganandan et al. [49] are shown in Table 3. Yoganandan et al. [50] also provided the failure deflection and force for adult C0-C2 segments as shown in Table 4. The normalized controlling points for the C0-C2 ligaments used the data in Table 3 and the corresponding ligaments are also shown in Table 4. These failure values were used to obtain the force-deflection curves for the child.

Since ligaments of children have different dimensions and properties, the following formulation was used to calculate the three controlling points of the force-deflection curve for pediatric ligaments. The data from Tables 3 and 4 were used.

$$\begin{cases} d_i = \varepsilon_{max} \times \left(\frac{\varepsilon_i}{\varepsilon_{max}}\right) \times l \\ f_i = \frac{F_{max} \times \left(\frac{F_i}{F_{max}}\right) \times \alpha_i \times \lambda_{iA}}{N_i} \end{cases} i = 1,2,3 \qquad (2)$$
$$\frac{\varepsilon_3}{\varepsilon_{max}} = 1; \quad \frac{F_3}{F_{max}} = 1$$

where d_i is the deflection for the child ligaments; l is the length of the ligaments in the child model; f_i is the force for the child ligament; α_i is the scaling factor of material property for ligaments which was 0.893; λ_{iA} is the scaling factor of sectional area that is defined as the square of the dimensional scaling factor G_S which was 0.723 (Table 1); N_i is the number of bar elements for each ligament in the child model; ε_1 is strain at point A; ε_2 is strain at point B; ε_{max} is failure tensile strain; F_1 is tensile force at point A; F_2 is tensile force at point B; F_{max} is failure tensile force. The lengths of upper ligaments reported by Panzer and Cronin [34] in the FE model were used to calculate the failure strains for the adult as shown in Table 4.

TABLE 3 Coefficients used to define ligament curves for adult [48,49]

	Point A		Point B		Point C			
					C2-C5		C6-C7	
	$\varepsilon_1/\varepsilon_{max}$	F_1/F_{max}	$\varepsilon_2/\varepsilon_{max}$	F_2/F_{max}	ε_{max}	F_{max} (N)	ε_{max}	F_{max} (N)
ALL	21.1%	10.8%	77.2%	85.9%	0.31	93	0.35	145
PLL	25.0%	9.8%	77.3%	77.9%	0.18	71	0.34	188
CL	26.0%	15.0%	76.0%	88.0%	1.48	120	1.16	181
LF	28.6%	20.9%	76.2%	89.3%	0.77	121	0.88	129
ISL	30.8%	20.1%	74.4%	90.9%	0.61	39	0.68	39

ε_1 strain at point A; ε_2 strain at point B; ε_{max} failure tensile strain; F_1 tensile force at point A; F_2 tensile force at point B; F_{max} failure tensile force

TABLE 4 Failure data for ligaments in C0 to C2 of adult [50] [34]

Spinal level	Type	F_{max} (N)	d_{max} (mm)	F-d laws	ε_{max}
OC-C1	JC	320	9.9	CL	2.54
OC-C1	AA-OM	232	18.9	ALL	0.68
OC-C1	PA-OM	83	18.1	LF	1.28
C1-C2	ALL	263	11.8	ALL	0.68
C1-C2	JC	314	9.3	CL	2.11
C1-C2	LF	111	9.6	LF	0.91
OC-C2	TM	76	11.9	PLL	0.41
OC-C2	Apical	214	8	ISL	0.36
OC-C2	Alar	357	14.1	ISL	2.20
OC-C2	CLV	436	12.5	CL	1.60

F_{max} failure tensile force; d_{max} failure tensile deflection; F-d laws the corresponding ligaments used to obtain the nomalized controlling points; JC joint capsules; AA-OM anterior atlanto-occipital membrane; PA-OM posterior atlanto±occipital membrane; ALL anterior longitudinal ligament; LF ligamentum-flavum; TM tectorial membrane; CLV cruciate ligament, vertical portion.

The thickness of the facet cartilages for the child was assumed to be 0.35 mm based on the thicknesses of facet cartilages for adults as reported by Yoganandan et al. [58]. The facet cartilage was modeled using hexahedral elements with an isotropic elastic material model [42]. The facet joint was treated as a contact problem using surface-to-surface contact with a friction coefficient of 0.1 [59]. Capsular ligaments were modeled using bar elements connecting the superior aspect of the facet joint to the inferior section.

The final cervical spine model including C1 to C7 is shown in Figure 3. In total, 578 1D bar elements, 19,992 2D quad shell elements and 20,172 hexahedral elements were used to construct the model. For the element sizes, 60.4% of all hexahedral elements were between 0.5-1.0 mm, 11.7% were between 1.0-1.5 mm, 0.1% were between 1.5-2.0 mm. and 27.8% were less than 0.5 mm with a minimum of 0.18 mm, which was used for modeling the thin growth plate.

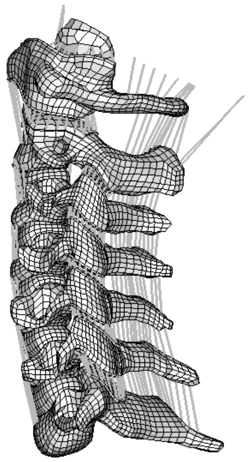

Figure 3: The ten-year-old FE neck model developed in this study

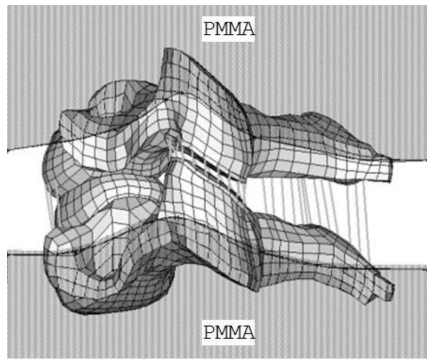

Figure 4: A schematic view of constrained area in segment tests (C4-C5).

Model validation

There are very few experimental data for child cervical spine published in the literature. Luck et al. [6,60,61] uniquely published a group of child neck tests in tension with ages ranging from 20 weeks gestational to 18 years. Three segments (Occipital-C2, C4-C5 and C6-C7) were tested in tension to determine the axial stiffness, displacements and forces at failure [6,60]. The experimental data of the nine-year-old and twelve-year-old subjects were used to validate the model since these two subjects were close to ten years of age. Responses of these three segments were simulated under tensile failure loads. For each simulation, a prescribed motion based on experimental data was applied to the superior nodes of the vertebral body in the direction of primary loading and the reaction force was calculated. The constrained area for the C4-C5 and C6-C7 segments is illustrated in Figure 4 according to the constrained method used in the tests [6] and communication with Dr. Luck. The superior nodes embedded in polymethylmethacrylate (PMMA) were loaded and the inferior ones were fixed. For C0-C2 segment simulation, since the head was not modeled in the present study and the head was fixed in the tests, the nodes that connected to the occipital bone were constrained in all degrees of freedom. The load was applied to the inferior nodes embedded in PMMA for the three segments respectively. Simulations were conducted using LS-DYNA version 971 (LSTC, Livermore, CA).

It was also revealed that child spinal ligaments could withstand significant stretching without tearing [4]. However, the values of failure strain are not directly reported in the literature. The stresses of intervertebral disc failure also needed to be identified. As such, a design of computer experiments (DOCE) was used to analyze the effect of ligamentous failure strain and intervertebral disc failure stress to the ultimate displacement and force in tension. DOCE was used to study the effect of such factors [62]. Four levels for increased strain by percentage were selected (0%, 25%, 50% and 75%) based on published studies [18,60]. Based on calculated failure stresses for intervertebral discs listed in Table 2, seven levels for failure stresses, ranging from 15 to 45 MPa, were used. Four failure strain and seven failure stress levels were assumed for the C4-C5 and C6-C7 segments. For a full factorial analysis, these selections constitute 56 simulations. Additionally, four levels of ligamentous failure strain were assumed for the C0-C2 segment. Altogether, a total of 60 runs were simulated in tension and the ultimate displacements and forces, identified from force-displacement curves, were used for DOCE analysis. The experimental ultimate displacement and force for a ten-year-old child were calculated by linear interpolation of the experimental values between the nine-year-old and twelve-year-old children. Minitab (Version, 15.0, State College, PA) was used to perform DOCE. Pareto and main effect charts were used to analyze the effects of these two factors [62]. In the Pareto chart, the horizontal bar shows the ranking of effects for each parameter and coupling. The main effect chart depicts the effects of each individual variable.

III. RESULTS

The simulated ultimate displacements and forces are shown in Figure 5. For the C0-C2 segment, the ultimate displacements and forces for tension increased as the ligament failure strain increased (Figure 5A). The simulated ultimate forces were within that of nine-year-old and twelve-year-old tests and smaller than that of calculated ten-year-old data, while all the simulated ultimate displacements were smaller than that of tests. The tensile stiffness was considered to determine the value of increased failure strain. The tensile stiffness was calculated using linear regression of the force-displacement curve between 10% and 90% of the failure force. The calculated stiffness values for the four runs (0%, 25%, 50% and 75%) were 324, 268, 218 and 200N/mm and the stiffness of the nine-year-old test was 219 N/mm. Thus, it is deemed that an increase of 50% for the failure strain of C0-C2 segment was appropriate.

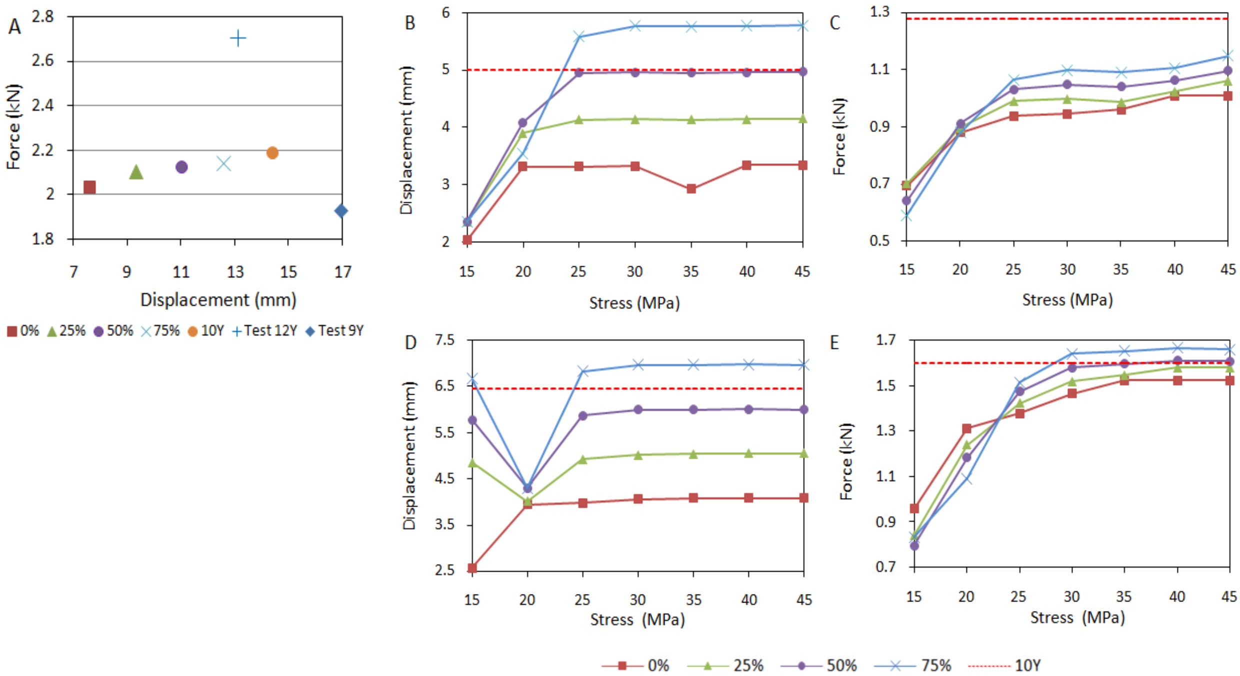

Figure 5: Ultimate displacements and forces in tension force-displacement curves for C0-C2 (A), C4-C5 (B, C) and C6-C7 segments (D, E). The abscissa (B-E) represents the disc failure stress and the ordinate represents the ultimate displacement (B, D) or ultimate force (C, E). 0%, %25, %50 and %75 were the increased percentages of assumed disc failure strains. The horizontal dashed lines represent the experimental ultimate displacement (B, D) or ultimate force (C, E) for ten-year-old child. The test values were obtained from Luck et al. (2013) and the ten-year-old child data were calculated using linear interpolation method.

For C4-C5 segment, Pareto's analysis (Figure 6) indicated that the ligament failure strain and intervertebral disc failure stress both affected the ultimate displacements significantly and only the failure stress affected the ultimate force in a statistically significant manner. Increasing the ligaments' failure strain percentage from 0% to 75% only increased the ultimate force by 0.1 kN (Figure 7). The disc failure stress could be determined based on the ultimate force and then the ligament failure strain could be determined based on the ultimate displacement. As shown in Figure 5C, when the disc failure stress was 30, 40 or 45 MPa for ligament failure strain of 50% or 75%, the ultimate force was close to experimental data. Considering that the calculated disc failure stress (Table 2) was between 29 and 36 MPa based on tests of Kasra et al. [55], the 30 MPa was selected. As shown in Figure 5B, when the ligament failure strain was 50% and disc failure stress was 30 MPa, the ultimate displacement was close to experimental data. Thus, the percentage of ligament failure strain was determined as 50%. For C6-C7 segment, the same relationship between disc failure stress and ligament failure strain was observed. As shown in Figures 5D and 5E, when the disc failure stress was larger than 30 MPa and the ligament failure strain was at the +50% level, the ultimate force and displacement were close to experimental data. Increasing the disc failure stress from 30 to 45 MPa, the tensile ultimate forces and displacements were almost the same. Considering that the calculated disc failure stress (Table 2) was 29.48 MPa based on tests of Kasra et al. [55], the 30 MPa was selected. Figure 8 shows the simulated tensile force-displacement curves using the determined disc failure stress and ligament failure strain.

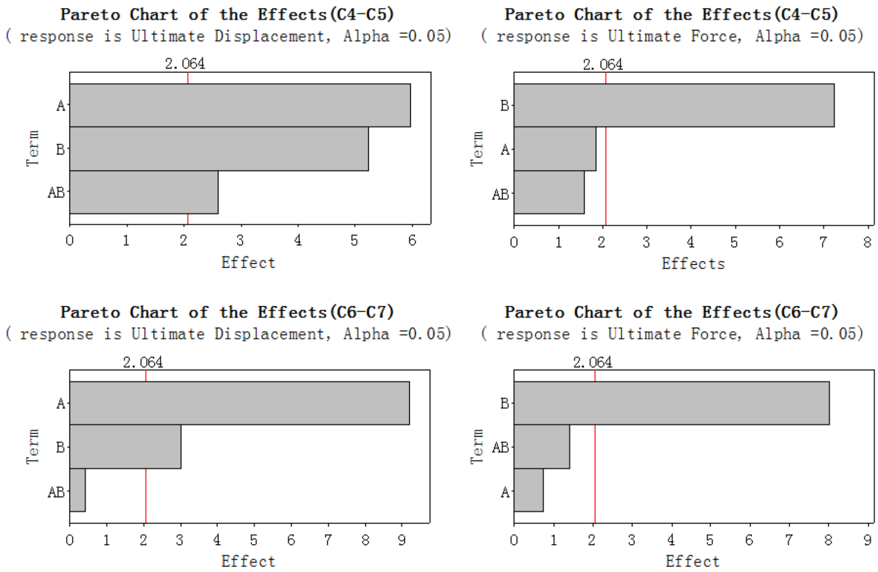

Figure 6: Pareto analysis for C4-C5 and C6-C7 segments (A: percentage increased for ligament failure strain, B: failure stress for intervertebral disc, and AB: combined effects)

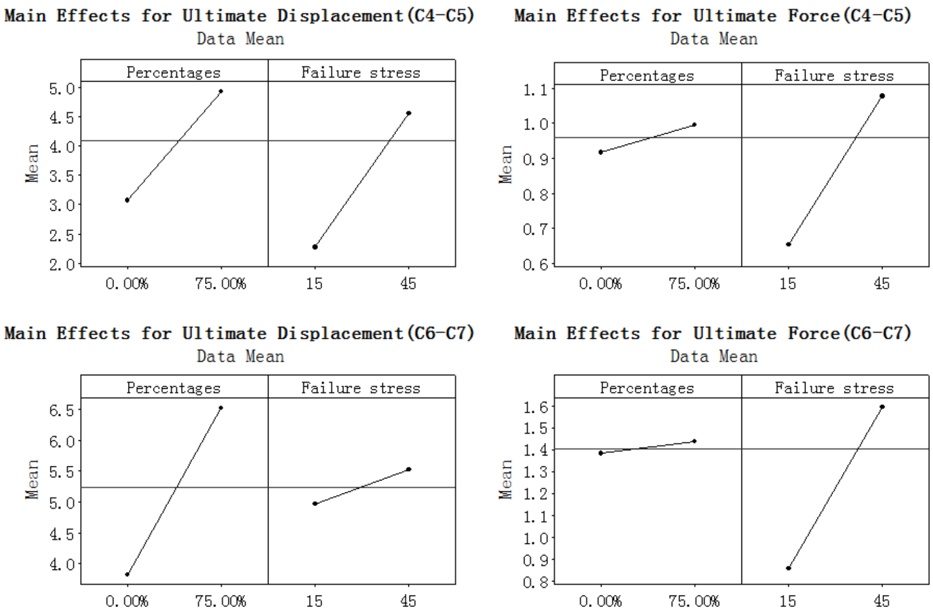

Figure 7: Main effects of the ultimate displacement-force of tension curves for C4-C5 and C6-C7 segments

The correlation and analysis (CORA) approach was used to evaluate the simulation curves against experimental data [63]. A correlation with a score of 0.7 or higher could be assumed as good [63]. For C0-C2 segment, the simulation curve was consistent with the experimental curve before the first experimental peak appeared (Figure 8A) (CORA score 0.89). The force at the first peak in simulation was 25.4% larger than that of the nine-year-old obtained experimentally. Additionally, the ultimate force predicted by the model was 6.6% larger than that measured from the nine-year-old. However, the model-predicted ultimate force was still less than that of the twelve-year-old test. The TM ligament failed initially and the ultimate force appeared when the JC ligament failed. After some ligament failures, the forces of other ligaments were still increased as the displacement increased. As a result, the force of the tension curve increased again after the ultimate force.

For C4-C5 segment, the simulation curve was consistent with the experimental curve before the first peak of the simulation curve appeared (Figure 8B) (CORA score 0.94). The ultimate force was 1.06 kN that was very close to the peak force of 1.05 kN measured from the nine-year-old subject. The simulated ultimate displacement was 5.0 mm, which was 23.0% larger than that reported for the nine-year-old, but the ultimate displacement was still within the experimental ranges. The intervertebral disc failed partially first followed by ligaments starting with PLL. The ultimate force appeared when ALL failed. ALL, PLL and LF bore similar forces when ligament failure initially occurred. The disc failed at the superior growth plate and endplate cartilage of C5.

For C6-C7 segment, the CORA score of the simulated curve before the ultimate force occurred was 0.65. The simulated ultimate force was 3.0% larger than that reported for the twelve-year-old and 7.0% smaller than that for the nine-year-old (Figure 8c). The simulated ultimate displacement was 7.9% larger than that of the twelve-year-old and 16.0% smaller than that of the nine-year-old. The intervertebral disc failed partially first followed by ligaments starting with PLL. The ultimate force appeared when PLL failed. ALL bore the largest force when ligament failure initially occurred. The disc failed at the inferior growth plate and endplate cartilage of C6.

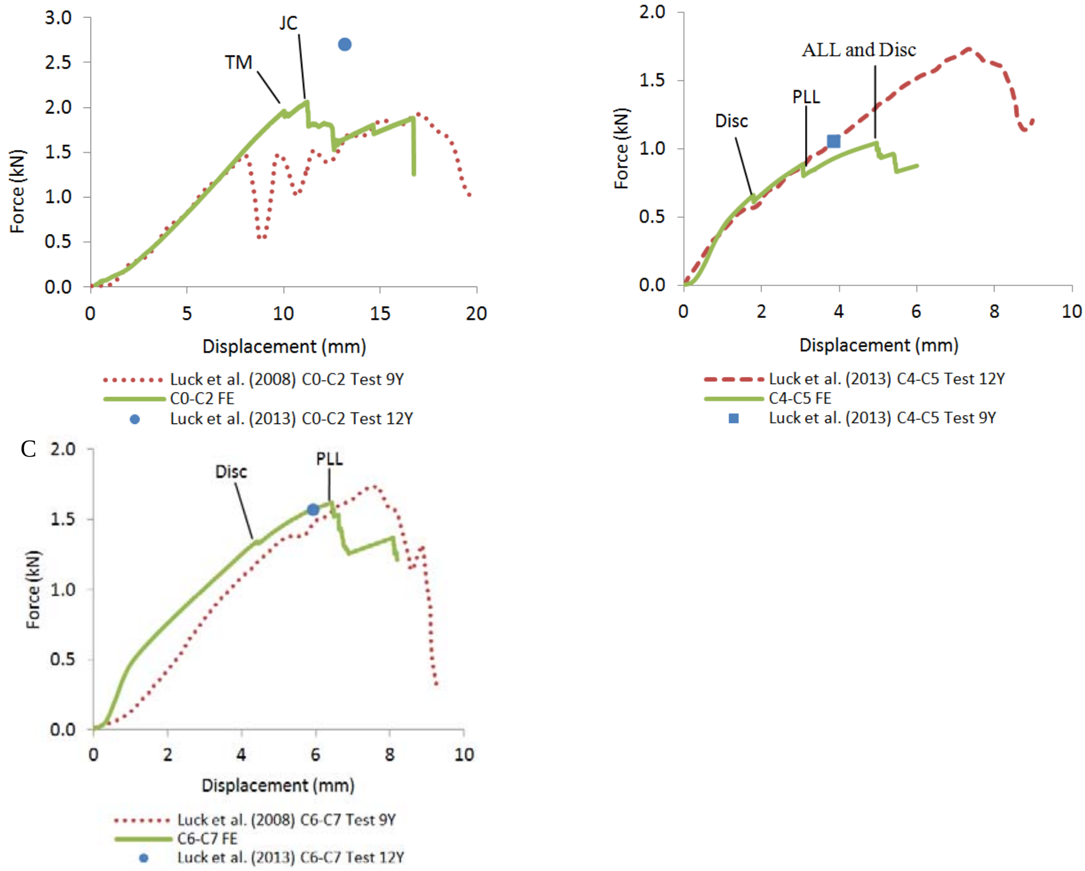

Figure 8: Tension response of simulation vs. children experimental data for the 9 years old and 12 years old at (A) C0-C2 segment, (B) C4-C5 segment, (C) C6-C7 segment. The initial failures occurred at tectorial membrane (TM) and joint capsules (JC) ligament for C0-C2 segment, and disc, PLL and ALL for C4-C5 segment, and disc and PLL for C6-C7 segment.

IV. DISCUSSION

A ten-year-old child cervical spine FE model was developed using detailed geometry of pediatric subjects and detailed material properties. The material properties were mostly obtained by scaling down adult experimental data using scaling factors based on published literature. The model was validated in tension against human cadaveric data. The failure response was validated in tension based on experimental force-deflection results.

The increased strains by percentage were determined using the DOCE analysis method. Dibb et al. [64] reported the ultimate displacements for adults were 10.8±3.9, 7.7±2, and 7.8±1.7 mm for C0-C2, C4-C5 and C6-C7 segments, respectively. The ultimate displacements for the nine-year-old and twelve-year-old child reported by Luck et al. [60] were within this deviation of adult results. In the current study, the failure displacements of ligaments did not exceed the values of the adult after increasing 50% of the failure strain.

For the intervertebral disc failure simulation, the element deletion method was used by defining a critical stress for the materials of the growth plate and endplate cartilage. DeWit and Cronin [54] defined the failure stresses based on the study of Kasra et al. [55]. The tension failure force and displacement fell outside the corridors reported by Dibb et al. [64]. It was assumed that the contact failure method caused the distinct results. The simulated ultimate forces and displacements for the current child model were consistent with experimental data. The element failure method, in fact, was better than the contact break method to define disc failure. The failure stress for C4-C5 and C6-C7 segments was 30 MPa which was close to the calculated failure stresses based on experimental data provided by Kasra et al. [55].

The DOCE results indicated that increasing the stress of the intervertebral disc failure did not increase the ultimate displacement or force when stress increased to a certain value (Figure 5). The reason may be that the peaks of the tension curves were controlled by ligaments. When a ligament failed, even though the intervertebral disc was not ruptured, the peak (drop of force) appeared in the tension curve. This could be proven by the tension results in Figures 8B and 8C. All the peaks of the curves appeared when ALL or PLL failed.

The model-predicted tensile force-displacement curves were compared with experimental data using the pre-determined failure strain for ligament and stress for disc (Figure 8). The failure initially occurred at the intervertebral disc, followed by PLL and ALL for the C4-C5 and C6-C7 segments. The same prediction was found in the study of DeWit and Cronin [54] who validated their adult FE C4-C5 segment model in tension. Injury descriptions for the neck segment due to tensile loading were provided by Luck [61]. Fractures of the dens and left condyle occurred for the C0-C2 segment; for the C4-C5 segment, the physis endplate failure occurred at C4 or C5; for the C6-C7 segment, the physis endplate failure occurred at C6 [61]. Similar failure locations in intervertebral discs for the C4-C5 and C6-C7 segments were found in the failure simulations. For the C0-C2 segment, the major failure force (first peak) was higher in the tensile simulation curve compared to experimental data (Figure 8a). The reason may be that bone failure was not considered in the current model but it was apparent in tests. The failure of bone (such as dens) might change the tensile force distribution to the ligaments.

As with most human models, limitations exist in this study. The primary ones are related to material properties and experimental data. Since there were no appropriate cadaveric material data for the child, the scaling method was used to get the material data for the child model. The accuracy of the scaling factors was also limited by the lack of material data. The experimental data used in tension validation came from only two specimens. Since no experimental data exist for validation, the bone failure was not considered in the current study.

V. CONCLUSIONS

Based on limited available child experimental data, a ten-year-old child FE cervical spine model was developed and validated. Advanced material models were used to define the material properties which were all based on existing literature. The element deletion method was used to simulate the disc failure. The failure properties of segmental cervical spine were validated based on published child cadaveric data. The failure strain of ligaments for the ten-year-old child was 50% larger than that of the adult and the failure stress for disc was found to be 30 MPa. It should be noted that only tension was simulated in the current study, which was the first step in developing a 10 YO child FE neck model. Future studies will include evaluation of responses of segment level in more loading scenarios and modeling of the full cervical spine with muscles.

VI. ACKNOWLEDGEMENT

The first author gratefully acknowledges the support from the China Scholarship Council (CSC) for the fellowship provided. The authors acknowledge Drs. Jason Luck and Roger Nightingale of Duke University for their help in describing experimental details. Finally, Toyota's Collaborative Safety Research Center funded Wayne State Bioengineering Center for the ten-year-old Finite Element Model development.

VII. REFERENCES

[1] Easter JS, Barkin R, Rosen CL and Ban K, Cervical Spine Injuries in Children, Part I: Mechanism of Injury, Clinical Presentation, and Imaging, *The Journal of Emergency Medicine,* 2011, 41(2):142-150.

[2] Cirak B, Ziegfeld S, Knight VM, Chang D, Avellino AM and Paidas CN, Spinal Injuries in Children, *J Pediatr Surg,* 2004, 39(4):607-612.

[3] Easter JS, Barkin R, Rosen CL and Ban K, Cervical Spine Injuries in Children, Part Ii: Management and Special Considerations, *The Journal of Emergency Medicine,* 2011, 41(3):252-256.

[4] McCall T, Fassett D and Brockmeyer D, Cervical Spine Trauma in Children: A Review, *Neurosurgical Focus,* 2006, 20(2):E5.

[5] Arlet V and Fassier F, The Pediatric Spine, *Lippincott Williams & Wilkins*, Philadelphia, 2001.

[6] Luck JF, Nightingale RW*, et al.*, Tensile Mechanical Properties of the Perinatal and Pediatric PMHS

Osteoligamentous Cervical Spine, *Stapp Car Crash Journal,* 2008, 52:107-134.
[7] Ouyang J, Zhu Q, Zhao W, Xu Y, Chen W and Zhong S, Biomechanical Assessment of the Pediatric Cervical Spine under Bending and Tensile Loading, *Spine,* 2005, 30(2)4:E716-723.
[8] Yoganandan N, Kumaresan S, Voo L and Pintar FA, Finite Element Applications in Human Cervical Spine Modeling, *Spine,* 1996, 21(15):1824-1834.
[9] Yang KH, Zhu F, Luan F, Zhao L and Begeman PC, Development of a Finite Element Model of the Human Neck, *42nd Stapp Car Crash Conference*, 1998, Tempe, Arizona, pp. 195-205.
[10] Zhang OH, Teo EC and Ng HW, Development and Validation of a C0-C7 FE Complex for Biomechanical Study, *Journal of Biomechanical Engineering,* 2005, 127(5):729-735.
[11] Kallemeyn N, Gandhi A, Kode S, Shivanna K, Smucker J and Grosland N, Validation of a C2-C7 Cervical Spine Finite Element Model Using Specimen-Specific Flexibility Data, *Med Eng Phys,* 2010, 32(5):482-489.
[12] Panzer MB and Cronin DS, C4-C5 Segment Finite Element Model Development, Validation, and Load-Sharing Investigation, *J Biomech,* 2009, 42(4):480-490.
[13] Kumaresan S, Yoganandan N, Pintar FA, Maiman DJ and Kuppa S, Biomechanical Study of Pediatric Human Cervical Spine: A Finite Element Approach, *Journal of Biomechanical Engineering,* 2000, 122(1):60-71.
[14] Kumaresan S, Yoganandan N and Pintar FA, Finite Element Analysis of the Cervical Spine: A Material Property Sensitivity Study, *Clin Biomech,* 1999, 14(1):41-53.
[15] Mizuno K, Deguchi T, Furukawa K and Miki K, Development of Three-Year-Old Child Human Fe Model, *Proceedings of IRCOBI Conference*, 2004, Graz, Austria, pp 335-336.
[16] Irwin A and Mertz H, Biomechanical Basis for the Crabi and Hybrid Iii Child Dummies, *41st Stapp Car Crash Conference*, 1997, pp. 261-272.
[17] Currey JD and Butler G, The Mechanical Properties of Bone Tissue in Children, *The Journal of Bone and Joint Surgery. American volume,* 1975, 57(6):810-814.
[18] Meyer F, Bourdet N, Roth S and Willinger R, Three Years Old Child Neck FE Modelling under Automotive Accident Conditions, *Proceedings of IRCOBI Conference*, 2007, Maastricht, Netherlands, pp. 277-289.
[19] Yoganandan N, Pintar FA, Kumaresan S and Gennarelli TA, Pediatric and Small Female Neck Injury Scale Factor and Tolerance Based on Human Spine Biomechanical Characteristic, *Proceedings of IRCOBI Conference*, 2000, Montpellier, France, pp. 345-359.
[20] Howarth CI, Routledge DA and Repetto-Wright R, An Analysis of Road Accidents Involving Child Pedestrians, *Ergonomics,* 1974, 17(3):319-330.
[21] Jonah BA and Engel GR, Measuring the Relative Risk of Pedestrian Accidents, *Accident Anal Prev,* 1983, 15(3):193-206.
[22] Wazana A, Krueger P, Raina P and Chambers L, A Review of Risk Factors for Child Pedestrian Injuries: Are They Modifiable?, *Injury Prevention,* 1997, 3(4):295-304.
[23] Jiang B, Cao L, Mao H, Wagner C, Marek S and Yang KH, Development of a 10-Year-Old Paediatric Thorax Finite Element Model Validated against Cardiopulmonary Resuscitation Data, *Comput Method Biomec,* 2012, Epub ahead-of-print, 1-13.
[24] Weber K, Lehman RJ and Schneider LW, Child Anthropometry for Restraint System Design, *University of Michigan Transportation Research Institure,* 1985, Ann Arbor, MI, Report No. UMTRI-85-23.
[25] Snyder RG, Anthropometry of Infants, Children, and Youths to Age 18 for Product Safety Design. Final Report, *Society of Automotive Engineers,* 1977, Warrendale, PA, SAE-SP 450.
[26] Agur AM and Dalley AF, Grant's Atlas of Anatomy, *Lippincott Williams & Wilkins*, Philadelphia, 2005.
[27] Moore KL and Dalley AF, Clinically Oriented Anatomy, *Lippincott Williams & Wilkins*, Philadelphia, 2006.
[28] Sairyo K, Goel VK*, et al.*, Three-Dimensional Finite Element Analysis of the Pediatric Lumbar Spine. Part I: Pathomechanism of Apophyseal Bony Ring Fracture, *European Spine Journal,* 2006, 15(6):923-929.
[29] Shivanna KH, Tadepalli SC and Grosland NM, Feature-Based Multiblock Finite Element Mesh Generation, *Computer-Aided Design,* 2010, doi:10.1016/j.cad.2010.07.005.

[30] De Santis G, De Beule M, Van Canneyt K, Segers P, Verdonck P and Verhegghe B, Full-Hexahedral Structured Meshing for Image-Based Computational Vascular Modeling, *Med Eng Phys,* 2011, 33(10):1318-1325.
[31] Mao H, Gao H, Cao L, Genthikatti V and Yang KH, Development of High-Quality Hexahedral Human Brain Meshes Using Feature-Based Multi-Block Approach, *Computer Methods in Biomechanics and Biomedical Engineering* 2011, Accepted. 10.1080/10255842.2011.617005.
[32] Grosland NM, Shivanna KH*, et al.*, Ia-Femesh: An Open-Source, Interactive, Multiblock Approach to

Anatomic Finite Element Model Development, *Comput Methods Programs Biomed,* 2009, 94(1):96-107.
[33] Gilsanz V, Perez FJ, Campbell PP, Dorey FJ, Lee DC and Wren TAL, Quantitative Ct Reference Values for Vertebral Trabecular Bone Density in Children and Young Adults, *Radiology,* 2009, 250(1):222-227.
[34] Panzer MB, Numerical Modelling of the Human Cervical Spine in Frontal Impact, MA.Sc, *University of Waterloo*, 2006.
[35] Panjabi MM, Chen NC, Shin EK and Wang JL, The Cortical Shell Architecture of Human Cervical Vertebral Bodies, *Spine,* 2001, 26(22):2478-2484.
[36] Mertz HJ, Jarrett K, Moss S, Salloum M and Zhao Y, The Hybrid III 10-Year-Old Dummy, *Stapp Car Crash Journal,* 2001, 45:319-328.
[37] Currey JD, Tensile Yield in Compact Bone Is Determined by Strain, Post-Yield Behaviour by Mineral Content, *J Biomech,* 2004, 37(4):549-556.
[38] Kopperdahl DL and Keaveny TM, Yield Strain Behavior of Trabecular Bone, *J Biomech,* 1998, 31(7):601-608.
[39] Cohen B, Chorney GS*, et al.*, The Microstructural Tensile Properties and Biochemical Composition of the Bovine Distal Femoral Growth Plate, *J Orthopaed Res,* 1992, 10(2):263-275.
[40] Fujii T, Takai S, Arai Y, Kim W, Amiel D and Hirasawa Y, Microstructural Properties of the Distal Growth Plate of the Rabbit Radius and Ulna: Biomechanical, Biochemical, and Morphological Studies, *J Orthopaed Res,* 2000, 18(1):87-93.
[41] Williams JL, Do PD, Eick JD and Schmidt TL, Tensile Properties of the Physis Vary with Anatomic Location, Thickness, Strain Rate and Age, *J Orthopaed Res,* 2001, 19(6):1043-1048.
[42] Yamada H, Strength of Biological Materials, *Williams & Wilkins*, Baltimore, 1970.
[43] Fujita Y, Duncan NA and Lotz JC, Radial Tensile Properties of the Lumbar Annulus Fibrosus Are Site and Degeneration Dependent, *J Orthopaed Res,* 1997, 15(6):814-819.
[44] Wagner DR and Lotz JC, Theoretical Model and Experimental Results for the Nonlinear Elastic Behavior of Human Annulus Fibrosus, *J Orthopaed Res,* 2004, 22(4):901-909.
[45] Iatridis JC, Setton LA, Foster RJ, Rawlins BA, Weidenbaum M and Mow VC, Degeneration Affects the Anisotropic and Nonlinear Behaviors of Human Anulus Fibrosus in Compression, *J Biomech,* 1998, 31(6): 535-544.
[46] Holzapfel GA, Schulze-Bauer CAJ, Feigl G and Regitnig P, Single Lamellar Mechanics of the Human Lumbar Anulus Fibrosus, *Biomech Model Mechan,* 2005, 3(3):125-140.
[47] Yang KH and Kish VL, Compressibility Measurement of Human Intervertebral Nucleus Pulposus, *J Biomech,* 1988, 21(10):865.
[48] Chazal J, Tanguy A*, et al.*, Biomechanical Properties of Spinal Ligaments and a Histological Study of the Supraspinal Ligament in Traction, *J Biomech,* 1985, 18(3):167-176.
[49] Yoganandan N, Kumaresan S and Pintar FA, Geometric and Mechanical Properties of Human Cervical Spine Ligaments, *Journal of Biomechanical Engineering,* 2000, 122(6):623-629.
[50] Yoganandan N, Kumaresan S and Pintar FA, Biomechanics of the Cervical Spine Part 2. Cervical Spine Soft Tissue Responses and Biomechanical Modeling, *Clin Biomech,* 2001, 16(1):1-27.
[51] Scifert JL, Biomechanical Investigations of the Lower Cervical Spine, *The University of Iowa,* 2000.
[52] Pooni JS, Hukins DW, Harris PF, Hilton RC and Davies KE, Comparison of the Structure of Human Intervertebral Discs in the Cervical, Thoracic and Lumbar Regions of the Spine, *Surgical and Radiologic Anatomy,* 1986, 8(3):175-182.
[53] Cassidy JJ, Hiltner A and Baer E, Hierarchical Structure of the Intervertebral Disc, *Connective tissue research,* 1989, 23(1):75-88.
[54] DeWit JA and Cronin DS, Cervical Spine Segment Finite Element Model for Traumatic Injury Prediction, *Journal of the Mechanical Behavior of Biomedical Materials,* 2012, 10:138-150.
[55] Kasra M, Parnianpour M, Shirazi-Adl A, Wang JL and Grynpas MD, Effect of Strain Rate on Tensile Properties of Sheep Disc Anulus Fibrosus, *Technology and Health Care,* 2004, 12(4):333-342.
[56] Yoganandan N, Pintar FA, Maiman DJ, Cusick JF, Sances A, Jr. and Walsh PR, Human Head-Neck Biomechanics under Axial Tension, *Med Eng Phys,* 1996, 18(4):289-294.
[57] Shim VPW, Liu JF and Lee VS, A Technique for Dynamic Tensile Testing of Human Cervical Spine Ligaments, *Exp Mech,* 2006, 46(1):77-89.
[58] Yoganandan N, Knowles SA, Maiman DJ and Pintar FA, Anatomic Study of the Morphology of Human Cervical Facet Joint, *Spine,* 2003, 28(20):2317-2323.
[59] Ueno K and Liu YK, A Three-Dimenstional Nonlinear Finite Element Model of Lumbar Intervertebral Joint in Torsion, *Journal of Biomechanical Engineering,* 1987, 109(3):200-209.

[60] Luck JF, Nightingale RW*, et al.*, Tensile Failure Properties of the Perinatal, Neonatal, and Pediatric Cadaveric Cervical Spine, *Spine,* 2013, 38(1):E1-E12.
[61] Luck JF, The Biomechanics of the Perinatal, Neonatal and Pediatric Cervical Spine: Investigation, Ph.D, *Duke University*, 2012.
[62] Mao H, Yang KH, King AI and Yang K, Computational Neurotrauma--Design, Simulation, and Analysis of Controlled Cortical Impact Model, *Biomech Model Mechan,* 2010, 9(6):763-772.
[63] Gehre C and Stahlschmidt S, Assessment of Dummy Models by Using Objective Rating Methods, *22nd International Technical Conference on the Enhanced Safety of Vehicles Conference (ESV)*, 2011, Washington D.C., USA, Paper 11-0216.
[64] Dibb AT, Nightingale RW, Luck JF, Chancey VC, Fronheiser LE and Myers BS, Tension and Combined Tension-Extension Structural Response and Tolerance Properties of the Human Male Ligamentous Cervical Spine, *Journal of biomechanical engineering,* 2009, 131(8), 081008.